Molecular dynamics simulation of interaction between nanorod and phospholipid molecules bilayer

Xin Wang(王鑫), Xiang-Qin Li(李香琴)†, Tian-Qing Liu(刘天庆)‡, Li-Dan Zhao(赵丽丹), Ke-Dong Song(宋克东), and Dan Ge(葛丹)

School of Chemical Engineering, Dalian University of Technology, Dalian 116024, *China*

(Received 13 February 2022; revised manuscript received 10 April 2022; accepted manuscript online 12 May 2022)

Natural and artificially prepared nanorods' surfaces have proved to have good bactericidal effect and self-cleaning property. In order to investigate whether nanorods can kill the enveloped virus, like destroying bacterial cell, we study the interaction between nanorods and virus envelope by establishing the models of nanorods with different sizes as well as the planar membrane and vesicle under the Dry Martini force field of molecular dynamics simulation. The results show that owing to the van der Waals attraction between nanorods and the tail hydrocarbon chain groups of phospholipid molecules, the phospholipid molecules on virus envelope are adsorbed to nanorods on a large scale. This process will increase the surface tension of lipid membrane and reduce the order of lipid molecules, resulting in irreparable damage to planar lipid membrane. Nanorods with different diameters have different effects on vesicle envelope, the larger the diameter of nanorod, the weaker the van der Waals effect on the unit cross-sectional area is and the smaller the degree of vesicle deformation. There is synergy between the nanorods in the nanorod array, which can enhance the speed and scale of lipid adsorption. The vesicle adsorbed in the array are difficult to desorb, and even if desorbed, vesicle will be seriously damaged. The deformation rate of the vesicle adsorbed in the nanorod array exceeds 100%, implying that the nanorod array has a strong destructive effect on the vesicle. This preliminarily proves the feasibility of nanorod array on a surface against enveloped virus, and provides a reference for the design of corresponding nanorods surface.

Keywords: nanorods surface, enveloped virus, lipids adsorption, vesicle deformation

PACS: 62.25.–g, 31.15.at, 42.62.Be **DOI:** 10.1088/1674-1056/ac6ed8

1. Introduction

In the past 20 years, there have been three fatal coronavirus outbreaks in human society. According to the investigation report issued by the World Health Organization, the severe acute respiratory syndrome coronavirus (SARS-CoV) infectious pneumonia in 2002 caused 8098 infections and 774 deaths, with a death rate of about 9.5%. The Middle East respiratory syndrome coronavirus (MERS-COV) pneumonia in 2012 caused 2494 infections and 858 deaths, with a mortality rate of about 34.4%. The severe acute respiratory syndrome coronavirus 2 (SARS-CoV-2) pneumonia has now caused hundreds of millions of people to be infected, millions of people to die, and now it is still spreading worldwide, which poses a serious threat to the health and life of all mankind.

Coronavirus is a kind of enveloped virus, with a protective envelope outside the virus nucleocapsid.[1,2] The envelope of the virus is a highly stable lipid bilayer vesicle. The previous studies have proved that the protective effect of lipid envelope on the virus is not weaker than that of protein shell.[3] And the rupture of lipid envelope will cause virus to die.[3] Enveloped viruses such as coronavirus represent a significant burden to human health around the world. One of the most important routes of transmission of viruses is through contacting virus-carrying materials.[4] According to the relevant studies, enveloped viruses have a strong ability to survive in vitro,[5] for example, coronavirus can remain active for 24 h on paperboard and survive for 2–3 days on plastic and stainless steel.[6] It means that enveloped viruses are more likely to infect humans through object contact. At present, chemical disinfectants are mainly sprayed on the surfaces of objects to cut off the route of virus transmission, but the extensive use of these chemical disinfectants will eventually bring serious pollution to the water and soil.[7] At the same time, indoor spraying will do harm to people's skins, mouths, noses, eyes, and other organs, and will also cause food pollution.[8] In addition, there is a hidden danger of fire. Therefore, it is necessary to explore effective physical sterilization and disinfection methods.

In recent years, the sterilization research on the surfaces with nanorods' structure has received more and more attention. Ivanova *et al*. first found that the nanorods structure on the wing surface of cicada or dragonfly has a good sterilization effect.[9,10] The nanorod structure induces the bacterial cell wall to deform to an extent beyond the allowable limit, causing the bacterial cell wall to rupture and deformation-mediated cell to die. It has been confirmed that the artificially prepared bionic nanorod structure surface such as silicon nanowire arrays and titanium-nanostructured surface also has excellent sterilization capability.[11–14] The mechanism of this nanos-

†Corresponding author. E-mail: xiangqinli@163.com
‡Corresponding author. E-mail: liutq@dlut.edu.cn

© 2023 Chinese Physical Society and IOP Publishing Ltd

tructure destroying bacterial cell wall is a simple mechanical effect rather than chemical effect,[15–17] and mammalian cells are usually not damaged.[18–20] Therefore, this sterilization method is safe, efficient, clean and harmless, and overcomes the difficulty that bacteria are easy to produce the drug resistance.

Viruses are very different from bacteria. Bacteria are protected by two layers of cell membranes and the cell wall with poor fluidity ($\sim$ 4-nm thick) between the two membranes.[21] And the diameter of bacterium is about several microns. But enveloped viruses are protected by a phospholipid bilayer membrane with high fluidity ($\sim$ 4-nm thick), with a diameter ranging from tens to hundreds of nanometers.[5,22] The size and diameter of the nanorods that kill bacteria are distributed between tens of nanometers and hundreds of nanometers, which even exceeds the diameter of some viruses. It is difficult to say that these nanorod structures that can kill bacteria can also kill viruses. At present, the research on nanostructure destroying virus is very few. In 2019, Cheeseman *et al*. explored the interaction between the nanostructures on the surface of dragonfly wings and the artificial lipid vesicles (DOPC) with a diameter of 3 μm experimentally, and proved that the nanostructures have the same destructive effect on high fluidity lipid membrane.[23] Besides, it has been proved that nanoparticles can irreversibly deform and kill the protein coat viruses and envelope viruses.[24–26] However, the damaging effect of nanorod on virus is rarely reported. Therefore, it is necessary to study the structural parameters of nanorods suitable for killing virus.

Molecular dynamics simulation (MD) has the advantages of low cost and high safety. With the ever-increasing computational power available and specialized hardware, it is now possible to simulate entire viruses, and to use such simulations to refine integrative models incorporating experimental data.[27,28] In recent years, it has been widely carried out to explore the interaction between nano materials and biofilm system, such as the damage of carbon nanotubes to animal cell membrane,[29–31] the interaction between nanoparticles and lipid membrane,[32–34] the damage of nano structure to bacterial cells.[21,35,36] Huber *et al*. established a complete coarsening model of flavivirus, including virus envelope and nucleocapsid, to explore the anti-envelope virus therapy according to the existing biophysical data.[28] Cagno *et al*. confirmed that the modified gold nanoparticles can kill HPV-16 virus by molecular dynamics simulation.[26] Dry Martini force field has been validated and widely used in lipid membrane simulations. Arnarez et al. proved that Dry Martini force field reproduces relatively well a variety of lipid membrane properties such as area per lipid, bilayer thickness, bending modulus, and coexistence of liquid-ordered and disordered domains.[37] Timr *et al*. also explored naturally hydrodynamic interactions in implicit solvent simulations of lipid systems through Dry Martini force fields.[38] Those work confirmed the reliability of the force field. However, the simulation of the mechanical interaction between nanorods and virus has not been reported to date.

In this work, through the method of coarse-grained molecular dynamics simulation (CGMD), the interaction between the biomimetic nanorod structure that can be artificially prepared at the present stage and enveloped virus is explored. The effect of size parameters of nanorod on the nano-level virus is investigated. If nanorod structure can damage virus, it will provide a new way for human beings to fight enveloped virus.

2. Calculation methods

2.1. Establishment of nanorod and virus envelope models

The nanorod model was constructed by using C5 beads in the Dry Martini force field developed by Arnarez *et al*.[37] This C5 bead is an almost neutral bead in the Dry Martini force field,[39] so the coarse-grained model can be used to represent nano materials with low toxicity to human body and high chemical stability. The C5 bead is often used to build coarse-grained models of stable elements such as gold due to their chemical stability in coarse-grained molecular dynamics simulation.[32,34] In this work, three different scales of nanorod models were constructed, which can be prepared in practical manufacture.[40,41] Their sizes are respectively 20 nm in diameter, 80 nm in height; 10 nm in diameter, 70 nm in height; 5 nm in diameter and 70 nm in height. The main part of the nanorod is a cylinder, and both ends are closed by a hemispherical structure as shown in Fig. 1(a). In addition, all the nanorods were hollowed out with a wall thickness of 2 nm. In this way, the amount of calculation can be reduced without affecting the simulation results.

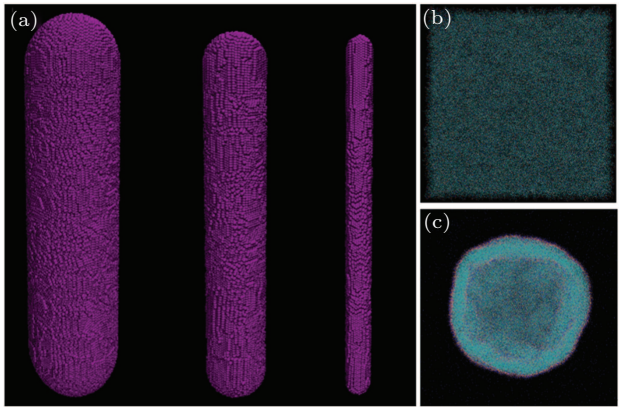


Fig. 1. Balanced models of three initial structures. (a) Nanorod models with different sizes: diameter 20 nm and height 80 nm, diameter 10 nm and height 70 nm, diameter 5 nm and height 70 nm; (b) planar phospholipid bilayer model; (c) phospholipid vesicle model.

Two kinds of lipid molecules, dipalmitoylphosphatidylcholine (DPPC) and palmitoyl-2-oleoyl-sn-glycero-3-

phosphogly-cerol (POPG), were used to establish the coating model of virus envelop (see detailes in supporting information). A planar phospholipid bilayer model and vesicle model were constructed through CHARMM-GUI.[42] The equilibrium models are shown in Figs. 1(b) and 1(c). The planar bilayer model consists of 8050 DPPC and 3450 POPG molecules, and two phospholipid molecular layers are symmetrically arranged with a size of 60 nm×60 nm×4.06 nm, showing negative electrical characteristics as a whole. In addition, the system also contains 3450 sodium ions to balance the charge of the system. The outer layer of the vesicle model contains 9636 DPPC and 4130 POPG molecules, and the inner layer includes 8603 DPPC and 3687 POPG molecules. There are 7817 sodium ions in the system to balance the charge of the system, with a specification of 54 nm×50 nm×56 nm irregular sphere. The relevant parameters of the viral envelope model come from the relevant data of COVID-19.[22,43,44] The details of nanorods, planar bilayer and vesicle model establishment, as well as the balance process and parameter settings, can be found from Figs. S1–S5 in supporting information.

2.2. System simulation parameter setting

Time steps of 40 fs were used to integrate the equations of motion. In all of the water-free simulations used is the second-order stochastic dynamics (SD) integrator in GROMACS with the friction in the Langevin equation and the time constant τ_t was set to be 4.0 ps. Unless specifically stated otherwise, the temperature was set to be 310 K as the default. And van der Waals interactions were smoothly shifted to zero between 0.9 nm and 1.2 nm, and coulomb interactions were screened by a relative permittivity constant, ε_r, of 15 and shifted to zero between 0.0 and 1.2 nm. This interaction scheme made both the potential and the forces vanish at the cutoff. The neighbor list was extended to 1.4 nm and updated every 10 steps. Periodic boundary conditions were adopted in the XY plane and Z direction.[37] And we used linear COM removal method to eliminate the overall translation phenomenon of the system, caused by periodic boundary calculation error, and updated every 10 steps.

All the simulations of the interaction between nanorod structure and phospholipid molecule bilayer in this work were equilibrium MD. Three systematic molecular dynamics simulations were carried out, including nanorod with a diameter of 20 nm and planar bilayer systems, nanorods of three sizes and vesicle, 2×2 array of nanorods with a diameter of 10 nm and vesicle system. Taking nanorod and planar membrane system-for example, the construction process was as follows: nanorod was added to the planar bilayer system and adjusted to the center of the plane membrane, and the energy minimization of the whole system was achieved by the steepest descent method. After that, the position restriction simulation of the system was carried out at 200 ns, and then the nanorod structure was fixed to imitate the fixed nanorods surface in reality and to maintain the rigidity of the nanorod structure. Through many attempts of centroid traction, the planar bilayer membrane and the nanorod reached the state of just contact, and then the traction was removed, so that the two can interact freely (The specific detail of the system construction are shown in the supporting information). Under the condition of NVT ensemble and 310 K, the system was formally simulated 3 μs. The establishment steps of nanorod and vesicle system were the same as the above, but the simulation time was set to be 4 μs.

Two repeated simulations under the same initial structure and simulation conditions were conducted. We repeatedly calculated the quantitative parameters such as the number of phospholipid molecules adsorbed and the sizes of pores in the three trajectories, and used the average value to eliminate the accidental simulation error.

All simulations in this paper were performed with GROMACS2018.4 software package,[45] and VMD1.9.3 was used for observation.[46]

3. Results and discussion

3.1. Interaction between nanorods and planar envelope

By analyzing the RMSD curve in the simulation process and the further running results of system at 3 μs (see detailes in supporting information), it is shown that when the simulation proceeded 3 μs, the system of nanorod and planar bilayer reached equilibrium. The morphological changes of the system during the simulation are shown in Fig. 2(a). Under the action of nanorod, the phospholipid molecules on the surface of the bilayer extract onto the nanorod, a total of 2256 lipid molecules are adsorbed on the nanorod, including 1559 DPPC and 697 POPG. This lipids extraction phenomenon generally occurs in the simulation of low charge hydrophobic or semi hydrophobic nanoparticles and lipid bilayer, and the particles will eventually stay in the hydrophobic tail hydrocarbon chain of lipid bilayer.[32,34,47] Jing and Zhu also confirmed this phenomenon experimentally.[48] As a result of lipid extraction, the upper and lower phospholipid molecular layers contacting the nanorods are separated from each other: the upper part of the nanorod is wrapped up by the upper phospholipid molecular layer, the phospholipid molecules on the lower layer adhere to the surface of the nanorod body, and extends downward. The average adsorption distance is about 18 nm. And the sinking distance of the planar bilayer is about 9 nm.

According to the radial distribution function of each lipid group around the nanorod (Fig. 2(c)), the nanorod is mainly wrapped by the hydrophobic tail hydrocarbon chain of the phospholipids. Because nanorod is far larger than nanoparticles, nanorod cannot be completely encased in planar bilayer phospholipids, but the scale of lipids extraction is far more

than that of nanoparticle systems. This makes the phospholipids between the extracted phospholipids and the planar bilayer body distributed sparsely and disorderly, and there are obvious structural defects (A region and B region in Fig. 2(b)). These areas are likely to be damaged already, and there are obvious gaps between the two phospholipid molecular layers in the main body of the membrane due to the separation of phospholipid molecular layers (region C in Fig. 2(b)). Because C5 beads are used to construct nanorod, the electrostatic interaction between nanorod and planar bilayer phospholipids can be ignored. In this paper, the changes of van der Waals potential and electrostatic potential between nanorods, phospholipid molecules, and sodium ions in the simulation process are analyzed. It is found that the LJ potential energy between nanorods and phospholipid molecules decreases, the LJ potential energy between phospholipid molecules increases, and the changes of other potential can be ignored. It is inferred that the van der Waals effect between nanorods and phospholipid molecules is the main driving force of lipid extraction process, while the van der Waals effect between phospholipids plays a main obstacle role. It can be seen from the overall LJ potential energy change curve between the nanorod and each phospholipid group and the LJ potential energy change curve between the nanorod and the hydrocarbon chain group at the tail of the phospholipid (Fig. 2(d)), the van der Waals effect between the nanorod and the phospholipid bilayer is attractive. The LJ potential energy curve between nanorods and lipid is basically consistent with the LJ potential energy curve between nanorod and phospholipids tail hydrocarbon chain groups, indicating that the van der Waals effect between nanorod and tail hydrocarbon chains of phospholipids is the main driving force of phospholipids extraction.

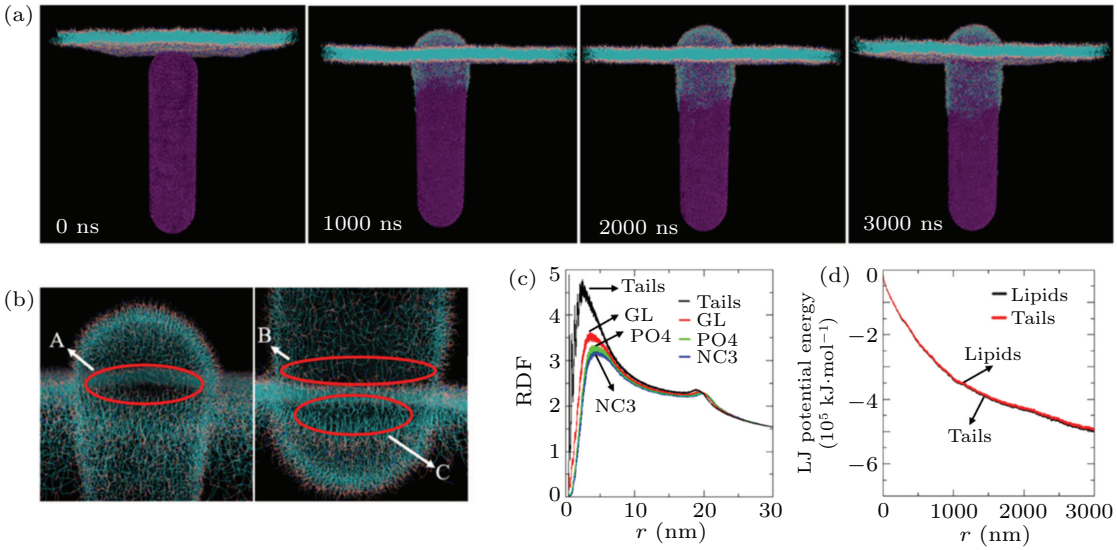


Fig. 2. Morphological changes of planar phospholipid bilayer interacting with nanorods. (a) Snapshots of nanorod and planar phospholipid bilayer system at different simulation times; (b) state of planar phospholipid bilayer at 3 μs; (c) radial distribution function of phospholipid groups around nanorod at 3 μs (NC3: nitrogenous bases groups in phospholipid, PO4: phosphate groups in phospholipid, GL: ester group in phospholipid, tails: hydrocarbon chain groups in phospholipid); (d) Lennard–Jone (LJ) potential energy changes of nanorod and all lipids, nanorod and tail hydrocarbon chain groups in simulation process (lipids: all groups in phospholipid).

In order to further explore the mechanism of damage of nanorod to planar bilayer, we carry out the recovery simulation of the planar bilayer. That is to remove the nanorod in the system at 3 μs, and then to continue simulating the planar bilayer under the same conditions. Owing to the high fluidity of the lipid membrane, the damage to the morphology of the bilayer will be spontaneously repaired. The recovery simulation reaches equilibrium at 100 ns, and the simulation process is shown in Fig. 3(a). During the recovery simulation, the separated phospholipid molecular layers are quickly recombined, however, holes are generated in areas A and B in Fig. 2(b) at the same time, and then these holes are also integrated into the membrane body with phospholipids. As more lipids return to the body of the plane bilayer, the area of the pores gradually decreases, but the plane bilayer cannot fully recover. Finally, a hole is left on the body of the plane bilayer. The maximum diameter of the hole in the XY plane direction is 17.1±2.5 nm×17.4±0.3 nm. The sterilization mechanism of nanorods is investigated with the finite element analysis,[49] it is found that the three-phase junction of nanorods, bacteria and the external environment is the place where bacteria are most stressed. The result obtained in this work is similar to it. Under the action of nanorod, region A (Fig. 2(b)) becomes the weakest part of the planar bilayer.

Furthermore, the lipid tail segmental order parameter of DPPC during the simulation of nanorod and planar phospholipid bilayer system (Fig. 3(b)) and the average surface tension of the planar phospholipid bilayer during the recovery process (Fig. 3(c)) are calculated. As we can see from the variation of the average lipid tail segmental order parameter, under the

action of nanorod, the average tail segmental order parameters of the two tail chains of DPPC decrease. The disorder of phospholipid molecules will severely impair the self-healing capability of the phospholipid bilayer. In the process of planar phospholipid bilayer recovery simulation, the initial average surface tension of the bilayer is 18 $mN{\cdot}m^{-1}$, and the average surface tension of the flat membrane is above 13 $mN{\cdot}m^{-1}$ at the first 5 ns, which is greater than the cleavage tension standard of animal cells, that is, 10 $mN{\cdot}m^{-1}$–12 $mN{\cdot}m^{-1}$.[50] Meanwhile, until the restoration simulation reaches equilibrium, the plane bilayer still has an average surface tension of 4 $mN{\cdot}m^{-1}$ and cannot be restored to the initial setting of 0 $mN{\cdot}m^{-1}$. This indicates that the surface tension of the plane bilayer has exceeded the normal range due to the lipids extraction of nanorod. In their study of the damage of carbon nanotubes to lysosomes, Zhu *et al*. found that even if the force of nanotubes on lysosomes cannot reach the cleavage tension standard, they will still destroy lysosomes under the action of carbon nanotubes for a long time.[31] There is no doubt that long time continuous high level of surface tension will cause serious damage to plane bilayer.

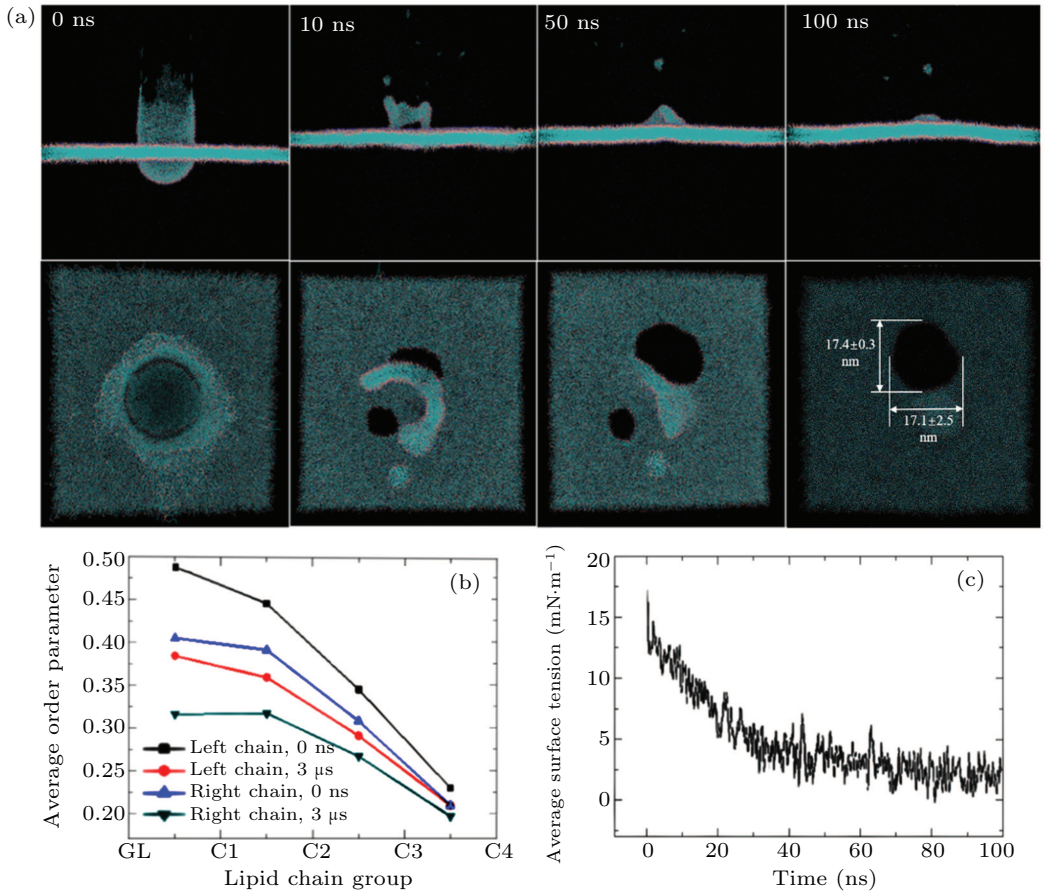


Fig. 3. Restoration simulation of planar phospholipid bilayer. (a) Simulation process of planar phospholipid bilayer restoration; (b) change of average lipid tail segmental order parameter of DPPC (DPPC tail chain beads: GL–C1–C2–C3–C4); (c) change of average surface tension of planar phospholipid bilayer during restoration simulation.

3.2. Interaction between single nanorod and vesicle

Because the morphology of vesicle is similar to that of the virus, the interaction between nanorod and vesicle is more consistent with the actual situation. Therefore, we further study the interaction between vesicle and nanorods with different diameters. Figure 4 shows the morphology change of the system and the magnified parts of the area of the vesicle contacting the 20-nm-, 10-nm-, and 5-nm-diameter nanorods at 4 μs. It can be seen that the nanorods of different sizes have distinct effects on vesicle. In terms of the morphological changes of versicle, the 20-nm-diameter nanorod only makes the vesicle shrink, while the 10-nm- and 5-nm-diameter nanorods more easily stretch the vesicle in the contact area, and make the vesicle present a "gourd" shape as a whole, Thus three layers of phospholipid molecular layers surround the nanorods at the local contact (Figs. 4(e) and 4(f)). We explore the degree of deformation by analyzing the overall and local displacement of vesicle along the nanorods. Since the nanorods remain fixed in the whole process, the change of the centroid distance between the vesicle and the nanorods can be regarded as the displacement of the vesicles as a whole. By making a comparison of the change curve of centroid distance between the vesicle and the nanorods of three diameters (see supporting information Fig. S9), it can be seen that

there is little difference among the displacements of the whole vesicle, caused by the three kinds of nanorods. Therefore, the deformation of vesicle, caused by nanorods with different diameters, is mainly reflected in local deformation. According to the sinking distances of the contact area of the vesicle along the nanorod (Figs. 4(d)–4(f)), the smaller the diameter of nanorods, the greater the local deformation of vesicle is.

In this work, the vesicle presents "gourd" shape under the action of 5-nm- and 10-nm-diameter nanorods, but this phenomenon does not appear under the action of 20-nm-diameter nanorod. This may be because the 5-nm- and 10-nm-diametyer nanorods have larger aspect ratios. The Zhu *et al*.'s simulation results[31] show that when the carbon nanotubes with a large aspect ratio, *i.e*., length exceeding the diameter of vesicle, were placed in lysosome, the shape of the lysosomal vesicle would become cherry shaped under the pressure of carbon nanotube. They found that the larger the aspect ratio of carbon nanotube, the greater the degree of deformation of the vesicle is.[31] In this work, the deformation of vesicles caused by 5-nm- and 10-nm-diameter nanorods are similar to the Zhu *et al*.'s results. However, the deformation of vesicle in this work is caused by the action of outside nanorod on vesicle, and the vesicle is attracted thus deforming through the van der Waals interaction between the nanorod and phospholipids.

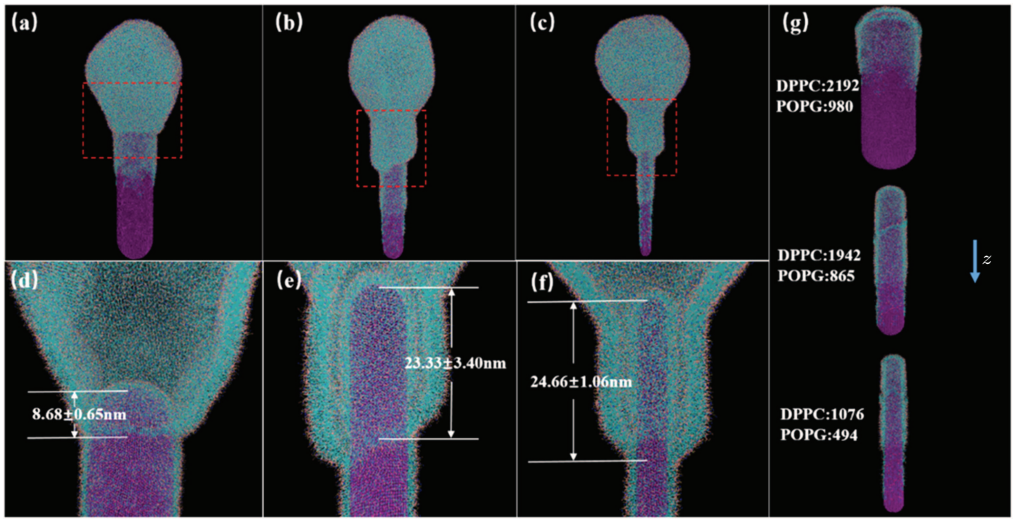


Fig. 4. Snapshots of nanorods with different sizes and vesicle system at 4 μs. [(a), (d)] diameter 20 nm; [(b), (e)] diameter 10 nm; [(c), (f)] diameter 5 nm; (g) lipids adsorbed on surfaces of nanorods.

Figure 5(a) shows the simulated time-dependent number of phospholipids adsorbed by the nanorods with three different diameters. The larger the diameter of the nanorods, the larger the area contacting the phospholipids is, the stronger the van der Waals effect, and thus the more the phospholipids adsorbed is. Interestingly, the change trend of the number of phospholipids adsorbed by the nanorods is the same as that of the LJ potential energy between the nanorods and phospholipids (see Fig. S9 in supporting information). It is also confirmed that the van der Waals interaction between nanorods and phospholipids is the main driving force of phospholipid adsorption. However, if we calculate the number of phospholipids adsorbed on the unit surface area of nanorods, the results are very different. Figure 5(b) shows the density distribution of phospholipids adsorbed on nanorods with different diameters along the Z axis at about 4 μs. It can be seen that the number of adsorbed phospholipids on the unit adsorption area of nanorods decreases with the increase of diameter although the total of adsorbed phospholipids increases. When the simulation reaches 4 μs, 3172 phospholipid molecules, including 2192 DPPC and 980 POPG molecules, are adsorbed on the surface of 20-nm-diameter nanorod, with an adsorbed density of 1.26 nm^{-2}; 2807 lipid molecules, including 1942 DPPC and 865 POPG molecules, are adsorbed on the surface of 10-nm-diameter nanorod, with an adsorbed density of 1.37 nm^{-2}; 1570 lipid molecules, including 1076 DPPC and 494 POPG molecules, are adsorbed on the surface of 5-nm-diameter nanorod, with an adsorbed density of 1.42 nm^{-2}. Therefore, the smaller the diameter of nanorod, the stronger the ability to adsorb phospholipids per unit surface area is. In addition, the ratio of DPPC to POPG is about 7:3, which also confirms that the electrostatic interaction between nanorod and phospholipids mentioned above is very weak, and it is not enough to adsorb more POPG molecules by Coulomb effect.

The depth of nanorods entering into vesicle (the distance from the top of nanorod to the separation of phospholipid bilayer at the contact site) in the simulation process is worked out, and the deformation rate of vesicle is calculated by the ratio of the distance of nanorod into vesicle to the original diameter of vesicle (Fig. 5(c)). In the initial stage of simulation, the nanorods with diameters of 10 nm and 20 nm have stronger ability to sdsorb the phospholipid than that with a diameter of 5 nm, so the penetration distance is larger and the vesicles are more likely to deform. However, the larger the

diameter of the nanorod, the greater the resistance to puncture into the vesicle is. After 1500 ns, the smaller the diameter of the nanorod, the greater the distance to puncture into the vesicle is. Although the nanorod with a diameter of 20 nm can still adsorb 800 phospholipid molecules after 2 μs, accounting for 1/4 of the total adsorbed phospholipids, it is difficult to continue to puncture into the vesicle, and the deformation degree of the vesicle basically does not change. The nanorods with a diameter of 10 nm and 5 nm, respectively, can still deform the vesicle strongly at 4 μs. At 4 μs, the penetration depths of nanorods with diameters of 20 nm, 10 nm, and 5 nm are about 8.68 nm (Fig. 4(d)), 23.33 nm (Fig. 4(e)) and 24.66 nm (Fig. 4(f)), and the corresponding vesicle deformation rates are 15.57%, 37.41%, and 41.29%, respectively. It shows that the deformation rate of vesicle increases with the decrease of nanorod diameter. This is consistent with the conclusion of previous studies on the sterilization mechanism of nanorods. That is, the smaller the diameter of nanorod, the higher the pressure on bacterial cell is and the shorter the time to reach the fracture strain.[16,49]

The LJ potential energy gradient between nanorods and vesicle along the height of nanorod in a unit cross-sectional area of nanorods is shown in Fig. 5(d), which exhibits the change of LJ potential energy with unit distance and unit cross-sectional area of nanorod penetrating into vesicle. We can see that the smaller the diameter of the nanorod, the stronger the LJ potential energy gradient acting on the vesicle by the nanorod is. This can also explain why the smaller the diameter of nanorod, the stronger the deformation of vesicle in the contact area is.

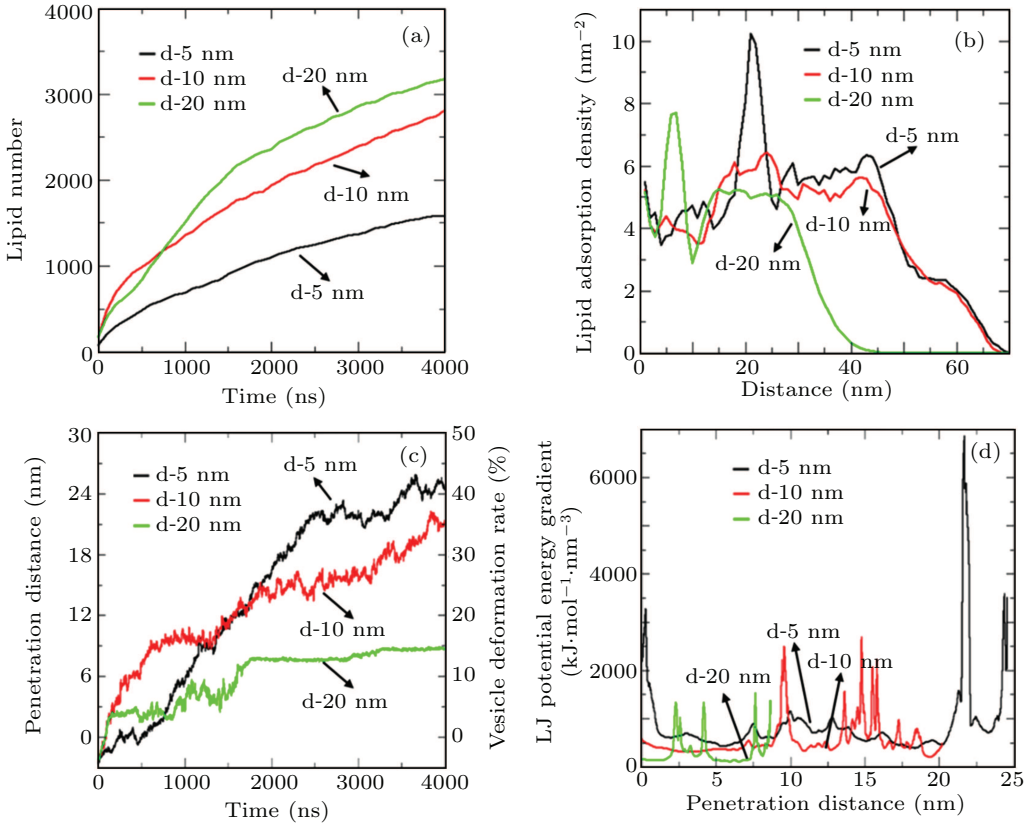


Fig. 5. Effects of nanorods on vesicle. (a) Simulated time dependent numbers of adsorbed lipids on three sizes of nanorods; (b) distance-dependent density distribution of phospholipids adsorbed on three sizes of nanorods at about 4 μs; (c) time-dependent penetration distances of nanorods of three different sizes into vesicle and vesicle deformation rate; (d) penetration-distance-dependent LJ potential energy gradient per unit cross-sectional area of nanorods of three different sizes.

3.3. Interaction between nanorod array and vesicle

In practical application, viral envelope will contact several nanorods on a surface with nanorod array. Therefore, we select four 10-nm-diameter nanorods to form 2×2 nanorods array, and simulate a vesicle for 4 μs. The position of nanorod array relative to vesicle is shown in Fig. 6(b). The center spacing of nanorod array is 20 nm, and the central axis of nanorod array coincides with the central axis of vesicle. The simulated vesicle deformation process is shown in Fig. 6(a). It can be seen that the vesicle gradually shrinks in the XY plane and gradually sinks into the nanorod gap along the Z direction. The nanorod array is completely wrapped in vesicle lipid molecules, and the vesicle deformation is very strong, causing a large area of phospholipid bilayer to be separated. The curve of the number of phospholipids adsorbed by the nanorod array varying with time is shown in Fig. 6(c). When simulating to 4 μs, 12940 phospholipid molecules are adsorbed on the surface of the nanorods, including 8955 DPPC and 3985

POPG. The number of adsorbed phospholipid molecules is about 4.5 times that of phospholipids adsorbed by a single 10 nm nanorod. This shows that there is a certain synergistic effect between the nanorods in the nanorod array, which strengthens the speed and scale of lipid extraction to a certain extent. The deformation rate of vesicle in the simulation process is shown in Fig. 6(d). Nanorod array is easier to penetrate into vesicle. The penetration depth and vesicle deformation rate are much higher than those under the action of a single nanorod. At 4 μs, the array penetrates into vesicles about 58.84 nm in depth, and the deformation rate of vesicles can reach 104%, far more than 45%, the cracking strain limit of bacterial cell.[51] Only a few kinds of microbes can withstand nearly 100% of the limit deformation, such as the influenza viruses that are rich in cholesterol and some giant single membrane vesicles (10 μm–50 μm) when they form a tether structure.[5,52] It is inferred that the vesicle envelope can be seriously damaged under the action of nanorod array. It can be seen that at 4 μs, the nanorods have raised the phospholipid bilayer at the top of the vesicle, and the array is completely wrapped in the vesicle phospholipid monolayer. At this time, the vesicle is firmly adsorbed in the nanorod array and is difficult to desorb.

Finally, the restoration simulation of desorbed vesicle was carried out (see supporting information, Fig. S10). The simulation method is similar to the recovery simulation of planar phospholipid bilayer. The simulation reached equilibrium after 300 ns. The results show that the desorbed vesicle remained in the tensile state and deforms seriously, and the previously isolated phospholipid monolayers were recombined and new small vesicles were formed in the vesicle. In addition, a large number of sodium ions in the vesicle leak out during this process, which proves that the desorbed vesicle has been irreversibly damaged.

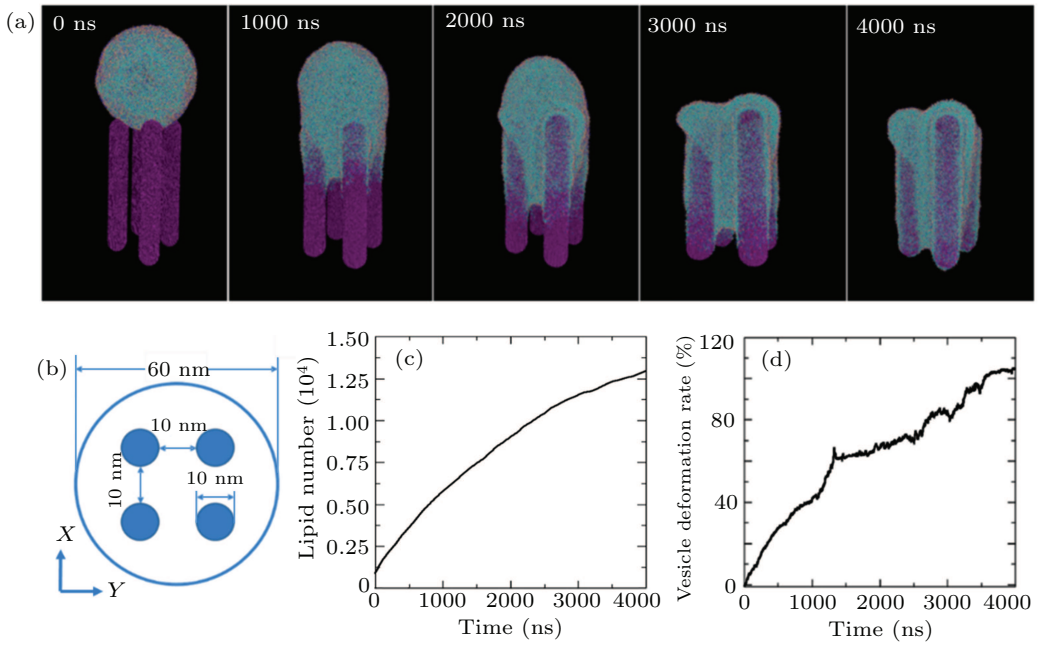


Fig. 6. Morphology changes of vesicle after its interaction with nanorod array. (a) Snapshots of nanorod array and lipid vesicle system at different simulation times; (b) schematic diagram of position of nanorod array relative to vesicle; (c) number of adsorbed lipids on nanorod array during simulation; (d) vesicle deformation rate caused by nanorod array.

4. Conclusions

In this work, we established the nanorods with different sizes, virus planar envelope and vesicle envelope models by coarse-grained simulation. Then, the interactions between nanorod and planar envelope and vesicle envelope were simulated under 310 K, NVT ensemble, and Dry Martini force field. The electrically neutral nanorods will not pierce the planar envelope nor the lipid membrane of vesicle, but be wrapped with the upper and lower phospholipid molecular layers through lipid extraction. This phenomenon will cause a large number of phospholipid molecules to leave the enveloped body, and form structural defects of phospholipid bilayer at the three-phase junction of nanorod, virus envelope body and external environment, which will damage the virus envelope. At the same time, nanorods will reduce the order of phospholipid molecules in phospholipid bilayer, and greatly increase the surface tension of virus envelope, which will weaken the self-healing capability of phospholipid bilayer. Nanorods with different diameters have different effects on virus vesicles. The smaller the diameter of nanorod, the more the phospholipids adsorbed on the unit surface area of nanorod is and the greater the van der Waals force per unit cross-sectional area of nanorod, and the easier the nanorod array penetrates the vesicle. Therefore, the smaller the diameter of nanorod, the more favorable it is to quickly destroy the en-

velope structure of the virus. The nanorod array can enhance the effect of lipid extraction, accelerate the adsorption and deformation process of virus envelope. The array can make the deformation rate of virus envelope exceed 100%, which means that it is difficult for virus to get away from the nanorod array. Therefore, the surface of nanorods has application value in the prevention of envelope viruses such as coronavirus.

Acknowledgement

Project supported by the National Natural Science Foundation of China (Grant No. 21676041).

References

[1] Barcena M, Oostergetel G T, Bartelink W, Faas F G A, Verkleij A, Rottier P J M, Koster A J and Bosch B J 2009 *Proc. Natl. Acad. Sci. USA* **106** 582
[2] Neuman B W and Buchmeier M J 2016 *Adv. Virus. Res.* **96** 1
[3] Garrido P F, Calvelo M, Blanco-Gonzalez A, Veleiro U, Suarez F, Conde D, Cabezon A, Pineiro A and Garcia-Fandino R 2020 *Int. J. Pharm.* **588** 119689
[4] Bchetnia M, Girard C, Duchaine C and Laprise C 2020 *J. Infect. Public Health* **13** 1601
[5] Li S, Eghiaian F, Sieben C, Herrmann A and Schaap I A T 2011 *Biophys. J.* **100** 637
[6] Doremalen N V, Bushmaker T, Morris D H, *et al.* 2020 *N. Engl. J. Med.* **382** 1564
[7] Zhang D, Chen L, Zang C, Chen Y and Lin H 2013 *Carbohydr Polym.* **92** 2088
[8] Yemiş F 2020 *Pakistan Journal of Analytical & Environmental Chemistry* **21** 179
[9] Ivanova E P, Hasan J, Webb H K, Truong V K, Watson G S, Watson J A, Baulin V A, Pogodin S, Wang J Y, Tobin M J, Lobbe C and Crawford R J 2012 *Small* **8** 2489
[10] Bandara C D, Singh S, Afara I O, Wolff A, Tesfamichael T, Ostrikov K and Oloyede A 2017 *ACS Appl. Mater. Interfaces* **9** 6746
[11] Ivanova E P, Hasan J, Webb H K, Gervinskas G, Juodkazis S, Truong V K, Wu A H, Lamb R N, Baulin V A, Watson G S, Watson J A, Mainwaring D E and Crawford R J 2013 *Nat. Commun.* **4** 2838
[12] Sengstock C, Lopian M, Motemani Y, Borgmann A, Khare C, Buenconsejo P J, Schildhauer T A, Ludwig A and Koller M 2014 *Nanotechnology* **25** 195101
[13] Susarrey-Arce A, Sorzabal-Bellido I, Oknianska A, McBride F, Beckett A J, Gardeniers J G E, Raval R, Tiggelaar R M and Diaz Fernandez Y A 2016 *J. Mater. Chem. B* **4** 3104
[14] Cui Q, Liu T, Li X, Song K and Ge D 2020 *ACS Appl. Nano Mater.* **3** 4599
[15] Xue F, Liu J, Guo L, Zhang L and Li Q 2015 *J. Theor. Biol.* **385** 1
[16] Liu T, Cui Q, Wu Q, Li X, Song K, Ge D and Guan S 2019 *J. Phys. Chem. B* **123** 8686
[17] Ivanova E P, Linklater D P, Werner M, Baulin V A, Xu X, Vrancken N, Rubanov S, Hanssen E, Wandiyanto J, Truong V K, Elbourne A, Maclaughlin S, Juodkazis S and Crawford R J 2020 *Proc. Natl. Acad. Sci. USA* **117** 12598
[18] Watson G S, Green D W, Schwarzkopf L, Li X, Cribb B W, Myhra S and Watson J A 2015 *Acta Biomater* **21** 109
[19] Tripathy A, Sen P, Su B and Briscoe W H 2017 *Adv. Colloid Interface Sci.* **248** 85
[20] Widyaratih D S, Hagedoorn P L, Otten L G, Ganjian M, Tumer N, Apachitei I, Hagen C W, Fratila-Apachitei L E and Zadpoor A A 2019 *Nanotechnology* **30** ab0a3a
[21] Hwang H, Paracini N, Parks J M, Lakey J H and Gumbart J C 2018 *Biochim. Biophys. Acta Biomembr.* **1860** 2566
[22] Zheng J 2020 *Int. J. Biol. Sci.* **16** 1678
[23] Cheeseman S, Truong V K, Walter V, Thalmann F, Marques C M, Hanssen E, Vongsvivut J, Tobin M J, Baulin V A, Juodkazis S, Maclaughlin S, Bryant G, Crawford R J and Ivanova E P 2019 *Langmuir* **35** 2422
[24] Bromberg L, Bromberg D J, Hatton T A, Bandin I, Concheiro A and Alvarez-Lorenzo C 2012 *Langmuir* **28** 4548
[25] de Souza E S J M, Hanchuk T D, Santos M I, Kobarg J, Bajgelman M C and Cardoso M B 2016 *ACS Appl. Mater. Interfaces* **8** 16564
[26] Cagno V, Andreozzi P, D'Alicarnasso M, Jacob Silva P, Mueller M, Galloux M, Le Goffic R, Jones S T, Vallino M, Hodek J, Weber J, Sen S, Janecek E R, Bekdemir A, Sanavio B, Martinelli C, Donalisio M, Rameix Welti M A, Eleouet J F, Han Y, Kaiser L, Vukovic L, Tapparel C, Kral P, Krol S, Lembo D and Stellacci F 2018 *Nat. Mater.* **17** 195
[27] Marzinek J K, Huber R G and Bond P J 2020 *Curr. Opin. Struct. Biol.* **61** 146
[28] Huber R G, Marzinek J K, Boon P L S, Yue W and Bond P J 2021 *Methods* **185** 28
[29] Kraszewski S, Bianco A, Tarek M and Ramseyer C 2012 *PLoS One* **7** e40703
[30] Lacerda L, Ali-Boucetta H, Kraszewski S, Tarek M, Prato M, Ramseyer C, Kostarelos K and Bianco A 2013 *Nanoscale* **5** 10242
[31] Zhu W, von dem Bussche A, Yi X, Qiu Y, Wang Z, Weston P, Hurt R H, Kane A B and Gao H 2016 *Proc. Natl. Acad. Sci. USA* **113** 12374
[32] Lin J, Zhang H, Chen Z and Zheng Y 2010 *Acs Nano* **4** 5421
[33] Yang K and Ma Y Q 2010 *Nat. Nanotechnol.* **5** 579
[34] Chen X, Tieleman D P and Liang Q 2018 *Nanoscale* **10** 2481
[35] Wu R, Ou X, Tian R, Zhang J, Jin H, Dong M, Li J and Liu L 2018 *Nanoscale* **10** 20162
[36] Roy S, Mondal A, Yadav V, Sarkar A, Banerjee R, Sanpui P and Jaiswal A 2019 *ACS Appl. Bio. Mater.* **2** 2738
[37] Arnarez C, Uusitalo J J, Masman M F, Ingolfsson H I, de Jong D H, Melo M N, Periole X, de Vries A H and Marrink S J 2015 *J. Chem. Theory Comput.* **11** 260
[38] A F B, Timr S, Melchionna S, Derreumaux P, Baaden M and Sterpone F 2019 *Sci. Rep.* **9** 16450
[39] Hardt S 2016 *Phys. Rev. E* **93** 052139
[40] Thai T, Zheng Y, Ng S H, Mudie S, Altissimo M and Bach U 2012 *Angew. Chem. Int. Ed. Engl* **51** 8732
[41] Martin A, Schopf C, Pescaglini A, Wang J J and Iacopino D 2014 *Langmuir* **30** 10206
[42] Qi Y, Ingolfsson H I, Cheng X, Lee J, Marrink S J and Im W 2015 *J. Chem. Theory Comput.* **11** 4486
[43] Earnest J T, Hantak M P, Park J E and Gallagher T 2015 *J. Virol.* **89** 6093
[44] Ke Z, Oton J, Qu K, Cortese M, Zila V, McKeane L, Nakane T, Zivanov J, Neufeldt C J, Cerikan B, Lu J M, Peukes J, Xiong X, Krausslich H G, Scheres S H W, Bartenschlager R and Briggs J A G 2020 *Nature* **588** 498
[45] Van Der Spoel D, Lindahl E, Hess B, Groenhof G, Mark A E and Berendsen H J 2005 *J. Comput. Chem.* **26** 1701
[46] Humphrey W F, Dalke A and Schulten K 1996 *Journal of Molecular Graphics* **14** 33
[47] Li Y, Chen X and Gu N 2008 *J. Phys. Chem. B* **112** 16647
[48] Jing B and Zhu Y 2011 *J. Am. Chem. Soc.* **133** 10983
[49] Cui Q, Liu T, Li X, Zhao L, Wu Q, Wang X, Song K and Ge D 2021 *Colloids Surf. B Biointerfaces* **206** 111929
[50] Hategan A, Law R, Kahn S and Discher D E 2003 *Biophysical Journal* **85** 2746
[51] Stocks S M and Thomas C R 2001 *Biotechnology and Bioengineering* **73** 370
[52] Bo L and Waugh R E 1989 *Biophysical Journal* **55** 509
[53] Rahaman O, Van Duin A C T, Goddard W A and Doren D J 2011 *J. Phys. Chem. B* **115** 249
[54] Best R B, Zhu X, Shim J, Lopes P E, Mittal J, Feig M and Mackerell A D 2012 *J. Chem. Theory Comput.* **8** 3257
[55] Humphrey W F, Dalke A and Schulten K 1996 *Journal of Molecular Graphics* **14** 33
[56] Lin J, Zhang H, Chen Z and Zheng Y 2010 *Acs Nano* **4** 5421
[57] Hardt S 2016 *Phys. Rev. E* **93** 052139
[58] Arnarez C, Uusitalo J J, Masman M F, Ingolfsson H I, de Jong D H, Melo M N, Periole X, de Vries A H and Marrink S J 2015 *J. Chem. Theory Comput.* **11** 260
[59] Qi Y, Ingolfsson H I, Cheng X, Lee J, Marrink S J and Im W 2015 *J. Chem. Theory Comput.* **11** 4486
[60] Nagle J F, Zhang R, Tristram-Nagle S, Sun W, Petrache H I and Suter R M 1996 *Biophysical Journal* **70** 1419
[61] Song B, Yuan H, Jameson C J and Murad S 2011 *Molecular Physics* **109** 1511